Research Square

Preprints are preliminary reports that have not undergone peer review.
They should not be considered conclusive, used to inform clinical practice,
or referenced by the media as validated information.

FGL2 Deficiency Attenuates Cisplatin-Induced Acute Kidney Injury and Associated Iron Dysregulation

Pan Xie
Southwest Hospital
Tian Wang
Southwest Hospital
Huan Chang
Southwest Hospital
Jingshuang Wang
The Second Affiliated Hospital of Chongqing Medical university
Yunfan Li
Chongqing University
Linxi Lv
Chongqing University
Wenzhan Xie
Chongqing University
Kanfu Peng
Southwest Hospital
Xiaohui Liao
The Second Affiliated Hospital of Chongqing Medical university
Claudio Ronco
cronco@goldnet.it

San Bortolo Hospital
Matteo Marcello
matteo.marcello@aulss8.veneto.it

San Bortolo Hospital
Hongwen Zhao
zhaohongwen@tmmu.edu.cn

Southwest Hospital

Research Article

Keywords: Cisplatin-induced acute kidney injury; Fibrinogen-like protein 2(FGL2); Iron homeostasis; Ferroptosis; Lysosomal alterations; LAMP1

Posted Date: November 24th, 2026

DOI: https://doi.org/10.21203/rs.3.rs-11834836/v1

License: This work is licensed under a Creative Commons Attribution 4.0 International License. Read Full License

Additional Declarations: The authors declare no competing interests.

FGL2 Deficiency Attenuates Cisplatin-Induced Acute Kidney Injury and Associated Iron Dysregulation

Pan Xie[1, 2†], Tian Wang[1, †], Huan Chang[1, 2,†], Jingshuang Wang[2],Yunfan Li[3], Linxi Lv[4], Wenzhan Xie[4] , Kanfu Peng[1] , Xiaohui Liao[2], Claudio Ronco[5,*], Matteo Marcello[5,*] , Hongwen Zhao[1*]

[1] Department of Nephrology, First Affiliated Hospital, Army Medical University, Chongqing 400038, China;

[2] Department of Nephrology, The Second Affiliated Hospital of Chongqing Medical University, Chongqing 401336, China;

[3] College of Bioengineering, Chongqing University, Chongqing 400044, China;

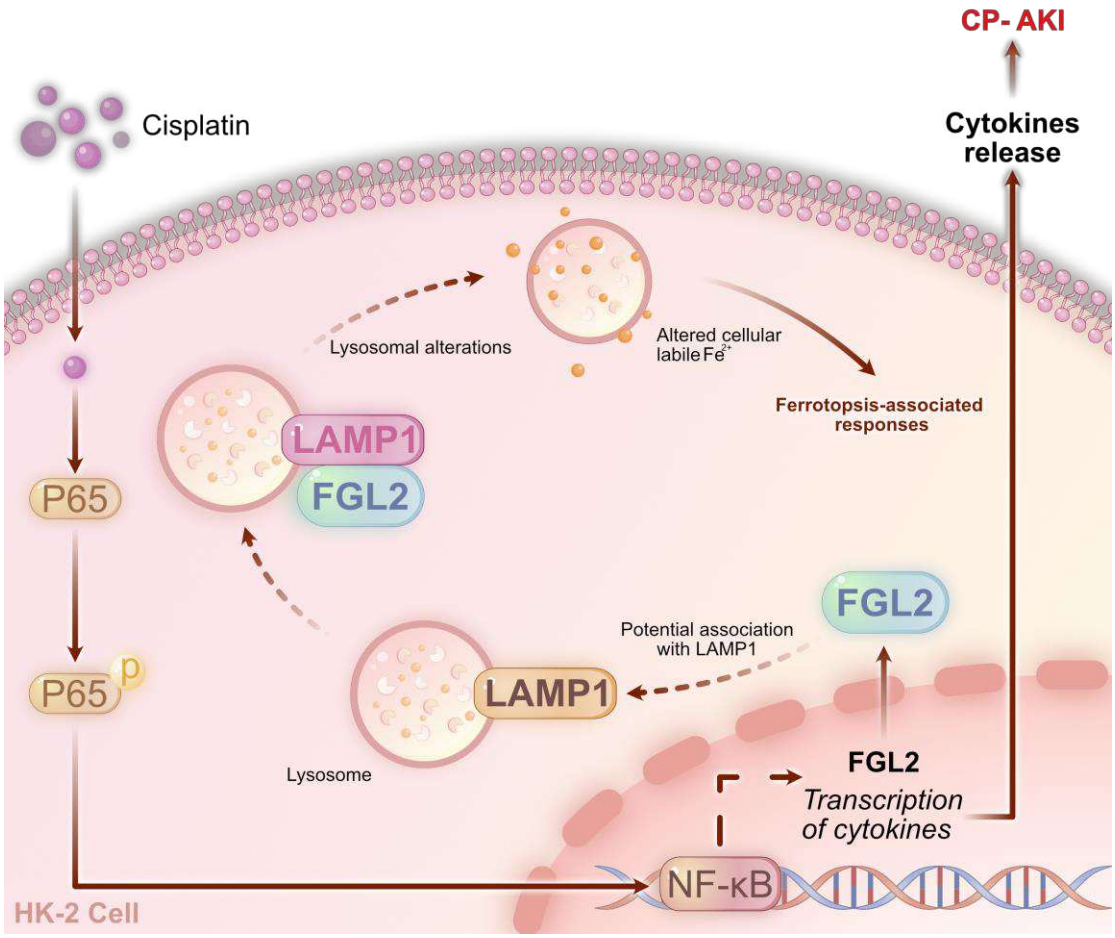
[4] School of Medicine, Chongqing University, Chongqing 400030, China;

[5] International Renal Research Institute of Vicenza (IRRIV), San Bortolo Hospital, Viale Rodolfi 37, 36100 Vicenza (VI), Italy.

E-mail address: xiepan@tmmu.edu.cn (P. Xie.),wangtian211002@163.com (T. Wang), changhuan0222@tmmu.edu.cn (H. Chang.), 273869578@qq.com (J. Wang)socomripeata@mail.com (Y. Li.), l18523921569@163.com (L. Lv), z577741395@163.com (W. Xie), 392906786@tmmu.edu.cn (K. P)，lxh@hospital.cqmu.edu.cn (X. L.)

Corresponding author's email address: cronco@goldnet.it (C. R.), matteo.marcello@aulss8.veneto.it (M. M.), Zhaohongwen@tmmu.edu.cn (H. Z.)

† These authors contributed equally to this work.



Graphic Abstract

Proposed model of FGL2-associated responses in cisplatin-induced acute kidney injury. Cisplatin exposure is associated with increased FGL2 expression, NF-κB activation, and inflammatory cytokine production. FGL2 deficiency or knockdown attenuates renal injury and several changes associated with oxidative stress, iron homeostasis, and ferroptosis. A potential association between FGL2 and LAMP1 may be involved in lysosomal alterations, although the underlying mechanism remains to be established. Dashed arrows indicate proposed relationships requiring further experimental validation.

Abstract

Cisplatin-induced acute kidney injury (CP-AKI) remains a major limitation of chemotherapy. Although fibrinogen-like protein 2 (FGL2) has been implicated in inflammatory responses, its involvement in cisplatin-related renal injury and iron homeostasis remains unclear. We investigated the role of FGL2 using cisplatin-treated wild-type and FGL2-knockout mice, together with human renal tubular epithelial (HK-2) cells subjected to FGL2 knockdown. Cisplatin increased FGL2 expression in renal tissues and HK-2 cells. FGL2 deficiency alleviated renal dysfunction and tubular injury in mice. In HK-2 cells, FGL2 silencing improved cell viability, reduced lipid reactive oxygen species and intracellular labile Fe^{2+} accumulation, and attenuated NF-κB activation. These changes were accompanied by partial preservation of GPX4 activity and altered expression of proteins involved in iron metabolism. FGL2 knockdown also mitigated cisplatin-associated changes in LAMP1 expression and lysosome-related markers. In separate experiments, LAMP1 modulation was associated with changes in lysosome-related markers, iron homeostasis, and cellular injury following cisplatin exposure. These results implicate FGL2 in cisplatin-induced renal injury and highlight its association with disturbances in iron homeostasis, lysosomal function, and ferroptosis-related cellular responses. The molecular relationship between FGL2 and LAMP1, however, remains to be established.

Keywords: Cisplatin-induced acute kidney injury; Fibrinogen-like protein 2 (FGL2); Iron homeostasis; Ferroptosis; Lysosomal alterations; LAMP1.

Abbreviations

Acute Kidney Injury (AKI)

Analysis of Variance (ANOVA)

Beta-Actin (β-actin)

Blood Urea Nitrogen (BUN)

Cell Counting Kit-8 (CCK-8)

Chromatin Immunoprecipitation (ChIP)

Chronic Kidney Disease (CKD)

Co-Immunoprecipitation (Co-IP)

Cisplatin (CP)

Cisplatin-Induced Acute Kidney Injury (CP-AKI)

Damage-Associated Molecular Patterns (DAMPs)

Dimethyl Sulfoxide (DMSO)

Dulbecco's Modified Eagle Medium (DMEM)

Enhanced Chemiluminescence (ECL)

End-Stage Renal Disease (ESRD)

Ethylenediaminetetraacetic Acid (EDTA)

Enzyme-Linked Immunosorbent Assay (ELISA)

Ferritin Heavy Chain (FTH1)

Ferroportin (FPN)

Ferrostatin-1 (Fer-1)

Fibrinogen (FIB)

Fibrinogen-Like Protein 2 (FGL2)

Fluorescein Isothiocyanate (FITC)

Glutathione (GSH)

Glutathione Peroxidase 4 (GPX4)

Human Proximal Renal Tubular Epithelial Cell Line (HK-2)

Horseradish Peroxidase (HRP)

Interleukin-1β (IL-1β)

Interleukin-6 (IL-6)

Interleukin-18 (IL-18)

Interquartile Range (IQR)

Kidney Injury Molecule-1 (KIM-1)

Lactate Dehydrogenase (LDH)

FGL2 knockdown lentivirus (Lv-shFGL2)

Empty vector controls (Lv-shNC)

Malondialdehyde (MDA)

Neutrophil Gelatinase-Associated Lipocalin (NGAL)

Nuclear Factor-κB (NF-κB)

Nuclear Receptor Coactivator 4 (NCOA4)

Optical Density (OD)

Oxidized Glutathione (GSSG)

PCDH Series Plasmids (PCDH)

Phosphate-Buffered Saline (PBS)

Phenylmethylsulfonyl Fluoride (PMSF)

Phosphorylated P65 (p-P65)

Platelet Factor 4 (PF4)

Polyvinylidene Difluoride (PVDF)

Prostaglandin-Endoperoxide Synthase 2 (PTGS2)

RAS Selective Lethal 3 (RSL3)

Reactive Oxygen Species (ROS)

Sodium Dodecyl Sulfate-Polyacrylamide Gel Electrophoresis (SDS-PAGE)

Serum Creatinine (Scr)

Small Interfering RNA (siRNA)

Solute Carrier Family 7 Member 11 (SLC7A11)

Tetramethylbenzidine (TMB)

Transmission Electron Microscopy (TEM)

Transferrin Receptor 1 (TfR1)

Tris-Buffered Saline with Tween 20 (TBST)

Tumor Necrosis Factor-α (TNF-α)

Tubulin Protein (Tubulin)

Wild-Type (WT)

1 Introduction

Cisplatin (CP) is widely used to treat solid tumors, but its clinical application is often limited by nephrotoxicity[1, 2]. Acute kidney injury (AKI) is among its most serious adverse effects and may require treatment interruption or dose adjustment[1]. Cisplatin accumulates in renal tubular epithelial cells, where it causes DNA damage, mitochondrial injury, oxidative stress, and inflammatory responses[1, 2]. These processes contribute to tubular dysfunction and the deterioration of renal function. Iron-dependent lipid peroxidation has also been implicated in cisplatin-induced AKI (CP-AKI)[3-5]. However, the contribution of ferroptotic cell death, particularly in cultured tubular epithelial cells, remains to be clarified[6].

Fibrinogen-like protein 2 (FGL2) participates in immune regulation and coagulation and has been linked to tissue injury in several disease settings[7]. Its role in AKI, however, appears to vary with the experimental model. Zhu et al. (2024) reported that global Fgl2 deletion aggravated cisplatin-induced renal injury and promoted pro-inflammatory macrophage polarization[8]. More recently, Yin et al. (2026) found that FGL2 contributed to the protective effects of irisin against ferroptosis in lipopolysaccharide-induced AKI[9]. These findings suggest that FGL2 may have context-dependent effects on renal injury, although the reasons for the differing observations remain unclear. Its relationship with iron homeostasis and intracellular stress responses during cisplatin exposure requires further investigation.

Lysosomes are involved in intracellular degradation, autophagy, and iron homeostasis[10, 11]. Disruption of lysosomal function can alter iron availability and cellular susceptibility to lipid peroxidation[11]. Lysosome-associated membrane protein 1 (LAMP1), an abundant lysosomal membrane glycoprotein, contributes to lysosomal homeostasis, including the regulation of luminal pH and degradative activity[12]. Recent evidence has also linked lysosomal damage to renal tubular injury following cisplatin exposure[13]. These observations raise the possibility that LAMP1-related lysosomal

changes may influence cellular responses to cisplatin. However, whether FGL2 is functionally associated with LAMP1 under these conditions remains unclear.

In this study, we examined the effects of FGL2 deficiency in a mouse model of CP-AKI and investigated FGL2 knockdown in human renal tubular epithelial HK-2 cells. We assessed renal injury, oxidative stress, iron metabolism, cell death-related responses, and lysosomal alterations. Protein docking, structural analyses, and experiments involving wild-type and mutant LAMP1 were used to explore a possible relationship between FGL2 and lysosomal homeostasis. We sought to clarify the role of FGL2 in cisplatin-induced renal injury and explore its potential association with LAMP1.

2 Materials and Methods

2.1 Bioinformatic Analysis

The RNA-sequencing dataset GSE106993 was obtained from the Gene Expression Omnibus (GEO). To assess transcriptional changes associated with cisplatin exposure, we selected eight mouse kidney samples without prior conditioning, comprising four vehicle-treated controls and four cisplatin-treated samples. Kidney tissues had been collected 72 h after injection.

The processed transcript-per-million (TPM) expression matrix was analyzed using R version 4.2.1. Expression values were transformed to $\log_2(\text{TPM} + 1)$, and differential expression was assessed with the limma package. P values were adjusted using the Benjamini–Hochberg method. Genes with an absolute $\log_2$ fold change greater than 1 and an adjusted P value below 0.05 were considered differentially expressed.

Gene Ontology (GO) and Kyoto Encyclopedia of Genes and Genomes (KEGG) enrichment analyses were performed using clusterProfiler, with adjusted $P < 0.05$ as the significance threshold. Gene set enrichment analysis (GSEA) was conducted using genes ranked by their moderated t-statistics. Differentially expressed genes were also compared with predefined mechanism-related gene sets to identify candidates for further investigation. Data visualization was performed using pheatmap and ggplot2.

2.2 Protein–protein interaction network and molecular docking analyses

A protein–protein interaction (PPI) network was generated using STRING to examine possible functional associations between FGL2 and proteins involved in lysosomal or autophagy-related processes. The minimum interaction score was set at 0.400, and disconnected nodes were excluded.

Predicted human FGL2 and LAMP1 structures were retrieved from the AlphaFold Protein Structure Database. Protein docking was carried out using HDOCK, with FGL2 and LAMP1 assigned as the receptor and ligand, respectively. The highest-ranked docking model was selected according to the HDOCK score and examined using PyMOL version 3.0.3 (Schrödinger, LLC). Candidate interface residues were identified from their spatial arrangement in the predicted complex. The docking results were used to guide subsequent structural analysis and did not establish direct protein binding.

2.3 Structural visualization and comparative docking of LAMP1 mutants

To examine the predicted FGL2–LAMP1 interface, serine 56 (S56), serine 69 (S69), and glutamate 81 (E81) of LAMP1 were selected for alanine substitution. A triple-mutant structural model (S56A/S69A/E81A) was generated and compared with wild-type LAMP1.

Both models were docked with FGL2 using HDOCK under identical settings. The highest-ranked complexes were visualized in PyMOL, with particular attention to the substituted residues and their surrounding interface regions. Differences between the predicted complexes were assessed qualitatively. These comparisons were considered exploratory and were not taken as evidence of changes in global protein conformation or binding affinity.

2.4 Circular dichroism spectroscopy

Circular dichroism (CD) spectroscopy was performed to compare the spectral characteristics of the indicated purified protein samples and their mixtures. Samples were prepared at matched concentrations in the same buffer, and far-UV spectra were recorded under identical conditions. Buffer spectra were subtracted to correct for background signals. The resulting spectra were compared to assess structural differences between the protein preparations. Measurements were independently repeated three times.

2.5 Cell culture and treatment

Human renal proximal tubular epithelial HK-2 cells were obtained from Army Medical University and maintained in HK-2 medium (Procell, Wuhan, China) supplemented with 10% fetal bovine serum and 1% penicillin–streptomycin at 37°C in a humidified atmosphere containing 5% CO_2.

For FGL2 knockdown, HK-2 cells were transduced with lentivirus expressing FGL2-targeting shRNA (Lv-shFGL2) or a negative-control shRNA (Lv-shNC). Following transduction, cells were treated with 40 μM cisplatin (CP) for 36 h. Cisplatin was freshly dissolved in sterile phosphate-buffered saline (PBS) and diluted in culture medium. Control cells received an equivalent volume of PBS. Four experimental groups were established: Lv-shNC + PBS, Lv-shNC + CP, Lv-shFGL2 + PBS, and Lv-shFGL2 + CP.

HEK293T cells used for lentiviral packaging were cultured in Dulbecco's modified Eagle medium (DMEM) supplemented with 10% fetal bovine serum and 1% penicillin–streptomycin under the same incubation conditions.

2.6 Plasmid construction

Full-length human LAMP1 cDNA was cloned into a mammalian expression vector to generate the wild-type LAMP1 construct. Based on the predicted docking interface, three residues (S56, S69, and E81) were individually substituted with alanine to generate the S56A, S69A, and E81A variants. A triple-mutant construct carrying all three substitutions was also prepared.

The mutations were introduced using overlap-extension PCR, and the resulting fragments were inserted into the same expression vector as wild-type LAMP1. All constructs were verified by DNA sequencing before use. Primer sequences are provided in the Supplementary Methods.

2.7 LAMP1 overexpression and mutant analysis

HK-2 cells were transfected with plasmids encoding wild-type LAMP1, the indicated LAMP1 mutants, or the corresponding empty vector using a transfection reagent according to the manufacturer's instructions. After transfection, cells were exposed to 40 μM cisplatin for 36 h. Expression of the introduced LAMP1 constructs was examined by Western blotting.

The effects of wild-type and mutant LAMP1 were evaluated by measuring lysosome-associated fluorescence, LC3 and p62 expression, intracellular labile Fe^{2+} levels, iron metabolism-related proteins, ROS generation, apoptosis, and NF-κB signaling. The treatment combinations used for individual experiments are shown in Figures 7 and 8.

2.8 Animal model and grouping

Male C57BL/6 wild-type (WT) and global Fgl2-knockout ($Fgl2^{-/-}$) mice, aged 6-8 weeks and weighing 20 ± 2 g, were obtained from Army Medical University. Animals were maintained under specific pathogen-free conditions at 22 ± 2°C and 55 ± 5% relative humidity, with a 12-h light/dark cycle and free access to food and water. Standard bedding, nesting materials, and shelters were provided.

Twenty mice were divided into four groups (n = 5 per group): WT + PBS, WT + CP, $Fgl2^{-/-}$ + PBS, and $Fgl2^{-/-}$ + CP. Cisplatin was dissolved in PBS and administered intraperitoneally at 20 mg/kg to induce AKI. Control animals received PBS. Within each genotype, animals were allocated to the treatment groups using a computer-generated randomization sequence.

No formal sample-size calculation was performed before the experiment. A group size of five mice was selected for this exploratory study. Serum creatinine, blood urea nitrogen, and histological tubular injury scores were used as the principal indicators of renal injury.

Animals were monitored at least daily for changes in body weight, activity, posture, appearance, food and water intake, and signs of distress. Humane endpoints included body weight loss exceeding 20%, inability to access food or water, persistent recumbency, severe lethargy, or unrelieved pain. No animals reached these endpoints before the scheduled termination of the experiment.

At 48 h after treatment, mice were deeply anesthetized with sodium pentobarbital (50 mg/kg, intraperitoneally). Blood was collected by cardiac puncture, followed by euthanasia through cervical dislocation. Death was confirmed before tissue collection. Serum was separated by centrifugation at 3,000 × g for 10 min at 4°C and stored at −80°C. Both kidneys were harvested. Samples intended for histological examination were fixed in 4% paraformaldehyde for 24h at 4°C, while the remaining tissues were used for biochemical analyses.

All animals completed the experiment, and no animals or data points were excluded. Treatment administration and sample collection were performed in an alternating order across groups to reduce potential order effects. Histological assessments were performed by investigators blinded to group allocation; other measurements and statistical analyses were not blinded.

All animal procedures were approved by the Laboratory Animal Welfare Ethics Committee of Army Medical University (Approval No. SYXK-2022-0018) and conducted in accordance with institutional guidelines for the care and use of laboratory animals.

2.9 Assessment of renal function

Serum creatinine (Scr) and blood urea nitrogen (BUN) concentrations were determined using commercial colorimetric assay kits (Jiancheng Bioengineering Institute, Nanjing, China) according to the manufacturer's protocols. Absorbance was measured with a microplate reader, and concentrations were calculated using the procedures provided with each kit. Additional assay details are provided in the Supplementary Methods.

2.10 Histological analysis

Kidney tissues were fixed in 4% paraformaldehyde at 4°C for 24 h, embedded in paraffin, and cut into 4-μm sections. Sections were stained with hematoxylin and eosin (H&E) to assess renal morphology.

Tubular injury was evaluated independently by two pathologists blinded to the experimental groups. The extent of brush-border loss, tubular dilation, and epithelial cell necrosis was graded using a five-point scale: 0, no injury; 1, <25%; 2, 25–50%; 3, 51–75%; and 4, >75% of tubules affected. Three randomly selected high-power fields were examined per section, with five mice analyzed in each group.

2.11 Western blot analysis

Total protein was extracted from HK-2 cells and mouse kidney tissues using RIPA lysis buffer supplemented with protease and phosphatase inhibitors. Protein concentrations were determined using a bicinchoninic acid assay. Equal amounts of protein were separated by SDS-PAGE and transferred onto polyvinylidene difluoride membranes.

After blocking, membranes were incubated overnight at 4°C with primary antibodies against KIM-1, NGAL, FGL2, GPX4, TfR1, FTH1, NCOA4, FPN, LAMP1, LC3, p62, p65, phosphorylated p65 (p-p65), BAX, and caspase-3, as appropriate. β-actin, GAPDH, or tubulin was used as the loading control. Membranes were subsequently incubated with horseradish peroxidase-conjugated secondary antibodies, and protein bands were visualized using enhanced chemiluminescence.

Band intensities were quantified using ImageJ and normalized to the corresponding loading controls.

2.12 GST pull-down assay

GST-tagged FGL2 and GST alone were immobilized on glutathione-conjugated beads and incubated separately with purified LAMP1 protein. After incubation, the beads were washed to remove unbound proteins, and the retained fractions were collected for Western blot analysis using antibodies against GST and LAMP1. GST alone served as a negative control to evaluate nonspecific protein retention.

2.13 RNA extraction and quantitative real-time PCR

Total RNA was extracted from HK-2 cells or mouse kidney tissues, and RNA concentration and purity were assessed spectrophotometrically. Equal amounts of RNA were reverse-transcribed into complementary DNA, followed by quantitative real-time PCR using SYBR Green chemistry.

GAPDH was used as the internal reference gene, and relative gene expression was calculated using the $2^{-}\Delta\Delta Ct$ method. Primer sequences are listed in Supplementary Table 2.

2.14 Measurement of intracellular ROS and lipid peroxidation

Intracellular reactive oxygen species (ROS) were measured using DCFH-DA (Beyotime, China). Following treatment, HK-2 cells were incubated with 10 μM DCFH-DA at 37°C for 30 min in the dark. Cells were then washed, collected, and resuspended in PBS. Fluorescence was measured by flow cytometry and analyzed using FlowJo.

Lipid peroxidation was assessed using C11-BODIPY 581/591 (Beyotime, China). Cells were incubated with 10 μM probe for 30 min at 37°C in the dark, washed with PBS, and examined by fluorescence microscopy. The ratio of oxidized green fluorescence to reduced red fluorescence was quantified using ImageJ.

2.15 Measurement of ferroptosis-related biochemical indicators

Following the indicated treatments, HK-2 cells were collected and lysed for biochemical analysis. Reduced glutathione (GSH), oxidized glutathione (GSSG), malondialdehyde (MDA), and glutathione peroxidase 4 (GPX4) activity were measured using commercial assay kits according to the manufacturers' protocols. PTGS2 protein levels were determined using a commercial quantitative assay kit and normalized to total protein content (pg/mg protein). The GSH/GSSG ratio was calculated from the measured concentrations. MDA levels and GPX4 activity were normalized to total protein content. Absorbance was measured at the wavelengths specified for each assay.

LAMP1-associated activity was assessed using a commercial assay kit according to the manufacturer's instructions. Following the indicated treatments, HK-2 cells were collected and processed for analysis. The assay signal was measured under the conditions specified by the manufacturer and expressed relative to the corresponding control group.

2.16 Measurement of inflammatory cytokines

Kidney tissues were homogenized in ice-cold PBS containing protease inhibitors and centrifuged at 10,000 × g for 15 min at 4°C. The resulting supernatants and serum samples were used for cytokine measurements.

The concentrations of IL-1β, IL-6, IL-18, and TNF-α were determined using commercial enzyme-linked immunosorbent assay (ELISA) kits according to the manufacturers' instructions. Absorbance was measured at 450 nm, and cytokine concentrations were calculated from standard curves. Five biological replicates were analyzed per group.

2.17 Cell viability assay

HK-2 cell viability was evaluated using the Cell Counting Kit-8 (CCK-8; Beyotime, China). Cells were seeded in 96-well plates at a density of 5×10^3 cells per well and

cultured overnight. Following treatment, CCK-8 reagent was added, and the plates were incubated at 37°C for 30 min.

Absorbance was measured at 450 nm. After subtraction of blank values, cell viability was expressed relative to the corresponding control group.

2.18 Flow cytometric analysis of apoptosis

Apoptosis was assessed by Annexin V and propidium iodide (PI) staining. Following treatment, HK-2 cells were harvested, washed twice with cold PBS, and resuspended in binding buffer. Annexin V and PI were added, and samples were incubated in the dark before flow-cytometric analysis.

Apoptotic cell populations were analyzed using FlowJo. The percentage of Annexin V-positive/PI-positive cells in the upper-right quadrant was used to quantify late apoptosis.

2.19 Evaluation of labile iron levels

Intracellular labile ferrous iron was assessed using FerroOrange (Beyotime, China). After treatment, HK-2 cells were incubated with 2 μM FerroOrange for 30 min at 37°C in the dark. Cells were subsequently washed with PBS and examined immediately by fluorescence microscopy.

Relative FerroOrange fluorescence intensity was quantified using ImageJ.

2.20 Assessment of lysosomal alterations

LysoTracker staining was used to examine lysosome-associated fluorescence in HK-2 cells. Following treatment, cells were incubated with LysoTracker at 37°C in the dark, washed with PBS, and imaged immediately. Fluorescence intensity and the number of LysoTracker-positive puncta were analyzed using ImageJ.

For FGL2 immunofluorescence staining, HK-2 cells were fixed with 4% paraformaldehyde, permeabilized, and blocked before incubation with an anti-FGL2 primary antibody overnight at 4°C. Cells were then incubated with a fluorescent secondary antibody, and nuclei were counterstained with DAPI. Fluorescence images were acquired under identical imaging conditions and analyzed using ImageJ.

2.21 Dual-Luciferase reporter assay for NF-κB activity detection

NF-κB transcriptional activity was assessed using a dual-luciferase reporter assay. HK-2 cells transduced with Lv-shNC or Lv-shFGL2 were co-transfected with an NF-κB-responsive firefly luciferase reporter plasmid and the pRL-TK Renilla luciferase control plasmid using Lipofectamine 3000.

Following transfection, cells were exposed to PBS or 40 μM cisplatin for 36 h. Firefly and Renilla luciferase activities were measured using a dual-luciferase reporter assay system according to the manufacturer's instructions. Relative NF-κB transcriptional activity was calculated as the ratio of firefly to Renilla luciferase activity. Each condition was assessed in technical triplicate, and the experiment was independently repeated three times.

2.22 Transmission Electron Microscopy Analysis of HK-2 Cell Ultrastructure

The ultrastructure of HK-2 cells was examined by transmission electron microscopy (TEM). Following treatment, cells were fixed, dehydrated, embedded, sectioned, and stained according to the procedure described in the Supplementary Methods.

Images were acquired using a Hitachi H-7650 transmission electron microscope. Five randomly selected fields per sample were examined for mitochondrial shrinkage, increased membrane density, and reduced or absent cristae.

2.23 Statistical analysis

Statistical analyses were performed using GraphPad Prism 9.0. Data normality was assessed using the Shapiro–Wilk test, and homogeneity of variance was evaluated using the Brown–Forsythe test. Normally distributed data are presented as mean ± standard deviation (SD), whereas non-normally distributed data are expressed as median with interquartile range (IQR).

Comparisons between two independent groups were performed using an unpaired two-tailed Student's t-test when the assumptions of normality and equal variance were met. Welch's t-test was applied to normally distributed data with unequal variances, and the Mann–Whitney U test was used for non-normally distributed data.

For comparisons involving more than two groups, one-way ANOVA followed by Tukey's multiple-comparison test was used when appropriate. Nonparametric multiple-group comparisons were performed using the Kruskal–Wallis test followed by Dunn's test. Experiments involving two independent factors, such as genotype and cisplatin treatment or FGL2 knockdown and cisplatin treatment, were analyzed using two-way ANOVA followed by Tukey's multiple-comparison test.

Pearson's correlation coefficient was used for normally distributed continuous variables, whereas Spearman's rank correlation was used when the assumptions for Pearson's

correlation were not met. Western blot bands and fluorescence intensities were quantified using ImageJ.

All statistical tests were two-sided, and $P < 0.05$ was considered statistically significant. Significance levels are indicated as follows: *$P < 0.05$, **$P < 0.01$, ***$P < 0.001$, and ****$P < 0.0001$.

In vitro experiments were independently repeated three to six times, with the exact number of independent experiments indicated in the corresponding figure legends. For animal experiments, five mice were included in each group, and each mouse was considered an independent biological replicate.

3 Results

3.1 Transcriptomic analysis identifies FGL2 as a candidate gene in CP-AKI

We analyzed the renal transcriptomic dataset GSE106993 to explore genes involved in cisplatin-induced acute kidney injury (CP-AKI) (Figure 1A). Cisplatin exposure was accompanied by widespread changes in gene expression (Figure 1B). Gene Ontology (GO) analysis highlighted processes involving vesicle transport, autophagy, and organelle organization, while Kyoto Encyclopedia of Genes and Genomes (KEGG) analysis identified pathways related to apoptosis, AMPK signaling, autophagy, and endocytosis (Figure 1C–D). Gene set enrichment analysis showed a positive enrichment score for apoptosis, but the result was not statistically significant (NES = 1.324, adjusted P = 0.251; Figure 1E).

Comparison of the differentially expressed genes with a predefined set of mechanism-related genes yielded eight overlapping candidates (Figure 1F). Among these, FGL2 was selected for further study because of its established roles in inflammation and coagulation.

We next examined the expression of these genes in kidneys from cisplatin-treated wild-type mice (Figure 1G). RT-qPCR revealed increased expression of Fgl2, Havcr1, Lcn2, Fth1, Sqstm1, Ncoa4, and Ftl1, whereas Gpx4 expression was reduced compared with controls (Figure 1H). The increase in renal Fgl2 expression following cisplatin exposure prompted us to investigate its contribution to kidney injury.

3.2 FGL2 deficiency attenuates cisplatin-induced renal and tubular cell injury

To examine the role of FGL2 in cisplatin-induced kidney injury, WT and $Fgl2^{-/-}$ mice were assessed 48 h after cisplatin administration (Figure 2A). Cisplatin caused marked tubular damage in WT mice, accompanied by increased histological injury scores, blood urea nitrogen, and serum creatinine levels. These changes were less pronounced in $Fgl2^{-/-}$ mice (Figure 2B–D). Western blot analysis showed increased renal FGL2, KIM-1, and NGAL expression after cisplatin treatment, whereas KIM-1 and NGAL

levels were lower in the knockout group (Figure 2E). FGL2 deficiency also reduced the cisplatin-associated increases in IL-1β, TNF-α, IL-6, and IL-18 (Figure 2F–I).

In HK-2 cells, FGL2 protein expression increased following cisplatin exposure, with the response varying according to drug concentration and treatment duration (Supplementary Figure 3A, B). We then examined the effects of FGL2 knockdown on cellular injury (Figure 3A). Cisplatin reduced cell viability and produced mitochondrial shrinkage and altered cristae morphology. FGL2 knockdown partially preserved viability and lessened these ultrastructural changes (Figure 3B, C).

Cisplatin exposure increased NF-κB transcriptional activity and p-p65 expression, both of which were reduced by FGL2 knockdown (Figure 3D, E). Intracellular ROS and lipid ROS levels followed a similar pattern (Figure 3F, G). MDA levels decreased following cisplatin exposure (Figure 3H), whereas PTGS2 levels increased and were reduced by FGL2 knockdown (Figure 3I). The cisplatin-associated reductions in the GSH/GSSG ratio and GPX4 activity were also partially reversed by FGL2 silencing (Figure 3J, K). Changes in PTGS2 and GPX4 mRNA expression were consistent with these broader cellular stress responses (Supplementary Figure 3E, F).

FerroOrange staining showed greater intracellular labile Fe^{2+} accumulation after cisplatin treatment, which was reduced by FGL2 knockdown (Figure 4A). Cisplatin also increased TfR1 and NCOA4 protein expression while decreasing FTH1 and FPN levels. FGL2 silencing partially reversed these alterations (Figure 4B). In parallel, cisplatin increased BAX and caspase-3 expression and the proportion of late apoptotic cells. FGL2 knockdown attenuated these protein changes and reduced the percentage of Annexin V/PI double-positive cells (Figure 4C, D).

These results indicate that FGL2 deficiency is associated with reduced cisplatin-induced renal injury and several cellular changes involving inflammatory signaling, oxidative stress, iron metabolism, and apoptosis.

3.3 FGL2 knockdown alters lysosomal and autophagy-related responses in cisplatin-treated HK-2 cells

Protein interaction network analysis identified potential associations between FGL2 and several lysosomal or autophagy-related proteins, including LAMP1, LAMP2, SQSTM1, and TFEB (Figure 5A). We therefore examined lysosome-associated fluorescence and autophagy markers in HK-2 cells exposed to cisplatin. FGL2-positive fluorescence increased after cisplatin treatment and was reduced by FGL2 knockdown. The number of LysoTracker-positive puncta also increased with cisplatin exposure and rose further in FGL2-silenced cells (Figure 5B).

Cisplatin increased LC3-II and p62 protein levels, whereas both were lower following FGL2 knockdown (Figure 5C). LAMP1 protein expression showed the opposite pattern, declining after cisplatin treatment and partially recovering in FGL2-silenced cells (Figure 5D). At the transcriptional level, cisplatin increased LC3 mRNA but reduced p62 and LAMP1 expression. These changes were partially reversed by FGL2 knockdown (Supplementary Figure 5A–C). Notably, the changes in p62 mRNA did not parallel those observed at the protein level.

To investigate a possible association between FGL2 and LAMP1, we performed GST pull-down and molecular docking analyses. LAMP1 was detected in GST-FGL2 fractions, but signals were also present in the GST-only controls (Figure 5E), preventing a definitive conclusion regarding specific binding. Docking analysis suggested a possible interaction interface between the two proteins (Figure 5F).

These observations link FGL2 knockdown to changes in lysosomal staining, autophagy-related proteins, and LAMP1 expression during cisplatin exposure. However, neither LysoTracker staining nor static measurements of LC3-II and p62 establish lysosomal membrane damage or altered autophagic flux. The proposed relationship between FGL2, LAMP1, and iron homeostasis is therefore presented as a working model (Figure 5G).

3.4 Structural analysis of a predicted FGL2–LAMP1 interface

Molecular docking was performed to explore a possible interaction between FGL2 and LAMP1. The predicted complex highlighted three candidate residues in LAMP1, E81, S56, and S69, located near the proposed interface (Figure 6A). These residues were selected for alanine substitution, either individually or in combination (Figure 6B). Comparative docking of wild-type and mutant LAMP1 revealed differences in the predicted interface arrangements (Figure 6C).

Circular dichroism spectra varied among the individual protein preparations and their mixtures (Figure 6D, E). Although these spectral differences may reflect changes in the structural properties of the tested samples, they do not establish direct binding between FGL2 and LAMP1. The LAMP1-associated assay readout decreased following cisplatin exposure and was partially restored by FGL2 knockdown (Figure 6F). No significant difference was detected between the wild-type and mutant LAMP1 groups under cisplatin treatment. The docking results identified candidate residues for further study, but the available experiments do not confirm a physical FGL2–LAMP1 interaction or demonstrate that FGL2 induces LAMP1 conformational changes. The proposed mechanism is illustrated in Figure 6G and remains to be experimentally validated.

3.5 LAMP1 modulation is associated with changes in cisplatin-induced cellular injury

To examine the effects of LAMP1 modulation during cisplatin exposure, HK-2 cells were subjected to FGL2 knockdown or transduced with constructs encoding wild-type or mutant LAMP1 in separate treatment groups (Figure 7A). Western blot analysis was used to assess LAMP1 protein expression under the indicated experimental conditions (Figure 7B).

LC3-II and p62 protein levels varied following LAMP1 modulation (Figure 7C). LysoTracker staining also differed between the groups, with more positive puncta in

cells expressing wild-type LAMP1 than in those expressing mutant LAMP1 (Figure 7D). Both LAMP1-modified groups showed reduced FerroOrange fluorescence compared with cisplatin-treated control cells, although the difference between wild-type and mutant LAMP1 was not significant (Figure 7E). Changes in TfR1, FTH1, NCOA4, and FPN protein expression were also observed, but their patterns did not consistently favor either LAMP1 construct (Figure 7F). RT-qPCR analysis revealed corresponding changes in lysosome-, autophagy-, and iron metabolism-related genes, without clear differences between the two LAMP1-modified groups (Supplementary Figure 6A–G).

We then assessed apoptosis and oxidative stress. BAX and caspase-3 protein levels were lower in both LAMP1-modified groups than in cisplatin-treated controls (Figure 8A). Both LAMP1-modified groups showed lower proportions of late apoptotic cells and reduced intracellular ROS signals (Figure 8B–D). Cell survival was higher in the LAMP1-modified groups than in the cisplatin-treated control group, although no significant difference was detected between wild-type and mutant LAMP1. Both interventions were associated with reduced p-p65 expression, with a lower level observed in the mutant group (Figure 8E). Changes in BAX, caspase-3, and p65 mRNA expression were also detected, without significant differences between the two LAMP1-modified groups (Supplementary Figure 7A–C).

Thus, modulation of LAMP1 expression was accompanied by changes in iron handling, lysosome-associated fluorescence, oxidative stress, and apoptosis during cisplatin exposure. These experiments, however, do not establish whether LAMP1 mediates the effects of FGL2. The proposed relationship remains to be tested using combined FGL2 and LAMP1 perturbations.

4 Discussion

Our experiments showed that FGL2 deficiency alleviated cisplatin-induced renal injury in mice, with lower levels of tubular damage, renal dysfunction, and inflammatory markers. FGL2 knockdown in HK-2 cells also reduced oxidative stress, intracellular iron accumulation, and apoptosis. These findings are relevant to the established involvement of tubular cell death and inflammatory signaling in cisplatin nephrotoxicity[14, 15]. Changes in lysosomal staining and autophagy-related proteins were observed alongside these effects, although the mechanisms connecting them remain uncertain.

Our observations contrast with previous reports on FGL2 in acute kidney injury. Zhu et al. found that global Fgl2 deletion aggravated cisplatin-induced renal injury and promoted pro-inflammatory macrophage polarization[8]. The opposing results are particularly noteworthy because both studies employed Fgl2-deficient mice in a cisplatin model. Several experimental conditions differed, including animal age and sampling time. Zhu et al. examined mice aged 8–10 weeks approximately 72 h after cisplatin administration, whereas we used 6-week-old mice with a 48-h endpoint. These differences may affect the injury phenotype but do not, by themselves, explain the discrepancy. Moreover, the earlier study emphasized macrophage responses, while our in vitro experiments focused on tubular epithelial cells. Because global Fgl2 deletion affects multiple cellular compartments, the contribution of individual cell populations remains unresolved. Yin et al. also reported that FGL2 was involved in the protective effects of irisin against ferroptosis in lipopolysaccharide-induced AKI[9]. Together, these studies point to a complex role for FGL2 in renal injury that may depend on the experimental setting and cellular context.

Evidence linking ferroptosis to cisplatin nephrotoxicity has accumulated over recent years. Ikeda et al. demonstrated that ferrostatin-1 and iron chelation alleviated renal injury in cisplatin-treated mice[3]. Hu et al. reported that vitamin D receptor activation

reduced cisplatin-associated ferroptotic injury partly through GPX4 regulation[16]. Protective effects involving iron metabolism and GPX4 have also been described following polydatin and valproic acid treatment [4, 17]. More recently, Xue et al. identified a role for TAZ in promoting cisplatin-induced tubular ferroptosis through GPX4-related regulation[18]. These studies provide functional evidence for ferroptosis in experimental CP-AKI, but do not establish that FGL2 regulates this pathway.

In our HK-2 model, FGL2 silencing reduced labile Fe^{2+} and lipid ROS accumulation while partially preserving the GSH/GSSG ratio and measured GPX4 activity. Changes in TfR1, FTH1, NCOA4, and FPN further indicated disturbances in iron handling. However, MDA measurements did not parallel the increase in lipid ROS following cisplatin exposure. The discrepancy remains unexplained and limits interpretation of lipid peroxidation across the different assays. Moreover, altered GPX4-related measurements, iron accumulation, and mitochondrial abnormalities cannot independently establish ferroptotic cell death[19]. The contribution of FGL2 to ferroptosis therefore requires direct functional confirmation.

FGL2 knockdown also reduced p65 phosphorylation and apoptosis following cisplatin treatment. Inflammatory signaling is an established component of cisplatin nephrotoxicity, with earlier work showing that TNF-α contributes to renal cytokine production and tissue injury[15]. Nevertheless, the present data cannot determine whether the changes in NF-κB signaling, iron metabolism, and apoptosis are causally connected. These responses may occur through overlapping or separate pathways, and their temporal relationships were not examined.

Lysosomal iron handling provides a possible link between the observed changes in autophagy-related proteins and cellular iron accumulation. Mancias et al. identified NCOA4 as a selective cargo receptor for ferritin degradation, establishing an important connection between autophagy and iron availability[20]. Subsequent studies showed that NCOA4-mediated ferritinophagy can promote ferroptosis by increasing the

618 intracellular labile iron pool[11, 21]. In renal tissue, autophagy has been shown to protect
619 against cisplatin-induced tubular injury, while more recent work demonstrated that
620 ESCRT III-mediated lysosomal repair can reduce renal tubular damage in experimental
621 CP-AKI [13, 22].

622 In our experiments, cisplatin increased LC3-II and p62 protein levels, reduced LAMP1
623 expression, and altered LysoTracker staining. FGL2 knockdown modified these
624 changes, including a further increase in LysoTracker-positive puncta. The biological
625 significance of this fluorescence pattern is uncertain because lysosomal staining can be
626 influenced by compartment abundance and acidity. Likewise, LC3-II and p62
627 measurements at a single time point cannot distinguish enhanced autophagosome
628 formation from reduced degradation[23]. The divergent patterns of p62 mRNA and
629 protein expression further limit interpretation. Dynamic assays would be needed to
630 determine whether FGL2 influences autophagic flux or lysosomal degradative capacity.

631 LAMP1 was examined as a candidate component of these lysosomal changes. Zhang
632 et al. demonstrated that LAMP1 and LAMP2 regulate lysosomal pH through their
633 interaction with TMEM175, providing evidence that these proteins participate directly
634 in lysosomal function[12]. Of particular relevance, Han et al. recently reported that FGL2
635 depletion promoted TFEB-dependent lysosomal degradation of PD-L1 through
636 modulation of mTORC1 signaling in hepatocellular carcinoma[24]. Although this study
637 was conducted in a different disease setting, it provides independent evidence linking
638 FGL2 to lysosome-related regulation. Whether a comparable relationship exists in renal
639 tubular epithelial cells remains unknown.

640 Our docking analysis identified a possible FGL2–LAMP1 interface involving LAMP1
641 residues E81, S56, and S69. However, structural predictions and differences in circular
642 dichroism spectra do not establish direct binding or FGL2-induced conformational
643 changes. LAMP1 was detected in the GST-FGL2 pull-down fraction, but its presence
644 in the GST-only control raises concerns about nonspecific retention. Thus, the current

evidence does not confirm a physical interaction between the two proteins.

The LAMP1 intervention experiments also require cautious interpretation. Changes in LAMP1 expression were accompanied by differences in lysosome-associated fluorescence, iron metabolism-related proteins, ROS, and apoptosis. Both wild-type and mutant LAMP1 groups showed improvements in several measurements, without a consistent advantage for either construct. Differences in protein abundance further complicate these comparisons. More importantly, LAMP1 modulation was not combined with FGL2 knockdown in an experimental design capable of establishing a downstream relationship. The data therefore support further investigation of LAMP1 during cisplatin injury but cannot identify it as a confirmed mediator of FGL2 activity.

Several limitations should be acknowledged. The animal experiments involved relatively few male mice, and global Fgl2 deletion prevented identification of the responsible cell population. The disagreement with previous studies remains unresolved. Most cellular experiments were performed in HK-2 cells, and the observations should be examined in additional renal tubular models. Direct functional evidence for FGL2-dependent ferroptosis is lacking, and the specificity of the GPX4 activity measurement requires verification. Lysosomal function and autophagic flux were not assessed dynamically, while the proposed FGL2–LAMP1 interaction requires more stringent biochemical validation. Combined FGL2 and LAMP1 perturbation experiments would be particularly valuable for testing whether these proteins act within the same injury pathway.

In summary, FGL2 deficiency was associated with reduced cisplatin-induced renal injury and changes in inflammatory signaling, oxidative stress, iron homeostasis, apoptosis, and lysosomal markers. The possible involvement of LAMP1 warrants further investigation, but the molecular relationship remains unconfirmed. Resolving the conflicting findings across AKI models will be important for establishing the role of FGL2 in renal injury.

672

5 Conclusions

FGL2 expression increased following cisplatin exposure, while Fgl2 deficiency alleviated renal dysfunction and tubular injury in mice. In HK-2 cells, FGL2 knockdown reduced oxidative stress, intracellular labile Fe^{2+} accumulation, and apoptosis, accompanied by changes in iron metabolism and ferroptosis-associated markers. Alterations in lysosomal staining and autophagy-related proteins were also observed. Molecular docking suggested a potential FGL2–LAMP1 interface, and LAMP1 modulation affected several cellular injury-related responses. However, the available evidence does not establish direct binding or a causal relationship between these proteins. Our findings implicate FGL2 in cisplatin-induced renal injury and highlight a possible link with iron homeostasis and lysosomal responses. Further investigation is required to clarify the underlying mechanisms and therapeutic relevance of FGL2.

Acknowledgements

We thank the staff of the Second Affiliated Hospital of Chongqing Medical University for their technical assistance. This study was supported by the Investigator-Initiated Trial Project (Grant No. 2024IITZDB08), the Natural Science Foundation of Chongqing, China (Grant No. CSTB2023NSCQ-MSX0570), and the Chongqing Appropriate Health Technology Promotion Project (Grant No. 2025JSTG031).

Conflict of Interest

The authors declare no conflict of interest.

Author contributions

P.X., T.W., and H.C. contributed equally to this study. P.X., T.W., and H.C. designed and performed the experiments, analyzed the data, drafted the manuscript, and prepared the figures. J.W., L.L., and W.X. assisted with animal experiments and sample detection. Y.L. performed the statistical analysis. K.P. provided experimental resources. X.L., C.R., M.M., and H.Z. supervised the project and critically revised the manuscript for important intellectual content. All authors discussed the results, reviewed the manuscript, and approved the final version.

Data Sharing Statement

The publicly available transcriptomic dataset analyzed in this study is available in the Gene Expression Omnibus under accession number GSE106993. All data supporting the findings of this study are included in the article and its Supplementary Information. Additional raw data are available from the corresponding author upon reasonable request. The data have not been deposited in a public repository because no additional large-scale dataset was generated in this study. No custom software or code was developed for this study.

Disclosure

All authors declare that they have no known competing financial interests or personal relationships that could have appeared to influence the work reported in this paper. This work was supported by [Chongqing Natural Science Foundation CSTB2023NSCQ-MSX0570, 2024IITZDB08 Investigator-Initiated Trial Project, 2025JSTG031 Chongqing Appropriate Health Technology Promotion Project]. The funders had no role in the design of the study; in the collection, analyses, or interpretation of data; in the writing of the manuscript; or in the decision to publish the results.

References

[1] OZKOK A, EDELSTEIN C L. Pathophysiology of cisplatin-induced acute kidney injury [J]. Biomed Res Int, 2014, 2014: 967826.

[2] MCSWEENEY K R, GADANEC L K, QARADAKHI T, et al. Mechanisms of Cisplatin-Induced Acute Kidney Injury: Pathological Mechanisms, Pharmacological Interventions, and Genetic Mitigations [J]. Cancers (Basel), 2021, 13(7).

[3] IKEDA Y, HAMANO H, HORINOUCHI Y, et al. Role of ferroptosis in cisplatin-induced acute nephrotoxicity in mice [J]. J Trace Elem Med Biol, 2021, 67: 126798.

[4] ZHOU L, YU P, WANG T T, et al. Polydatin Attenuates Cisplatin-Induced Acute Kidney Injury by Inhibiting Ferroptosis [J]. Oxid Med Cell Longev, 2022, 2022: 9947191.

[5] LAI K, CHEN Z, LIN S, et al. The IDH1-R132H mutation aggravates cisplatin-induced acute kidney injury by promoting ferroptosis through disrupting NDUFA1 and FSP1 interaction [J]. Cell Death Differ, 2025, 32(2): 242-55.

[6] DONG X Q, CHU L K, CAO X, et al. Glutathione metabolism rewiring protects renal tubule cells against cisplatin-induced apoptosis and ferroptosis [J]. Redox Rep, 2023, 28(1): 2152607.

[7] WANG C, SUN H, WANG R, et al. FGL2: A new target molecule for coagulation and immune regulation in infectious disease [J]. Int Immunopharmacol, 2024, 143(Pt 3): 113505.

[8] ZHU L, XU G, XIE P, PENG K. Role of Fgl2 in macrophage polarization during acute kidney injury in mice [J]. Journal of Army Medical University, 2024, 46(13): 1467–1476. doi:10.16016/j.2097-0927.202401019.

[9] YIN S, WANG Y, HUANG D, et al. Irisin alleviates ferroptosis in LPS-induced acute kidney injury via regulating FGL2 [J]. Toxicol Appl Pharmacol, 2026, 513: 117870.

[10] GROS F, MULLER S. The role of lysosomes in metabolic and autoimmune diseases [J]. Nat Rev Nephrol, 2023, 19(6): 366-83.

[11] GAO M, MONIAN P, PAN Q, et al. Ferroptosis is an autophagic cell death process [J]. Cell Res, 2016, 26(9): 1021-32.

[12] ZHANG J, ZENG W, HAN Y, et al. Lysosomal LAMP proteins regulate lysosomal pH by direct inhibition of the TMEM175 channel [J]. Mol Cell, 2023, 83(14): 2524-39 e7.

[13] TIAN Z, WU Y, YI B, et al. ESCRT III-mediated lysosomal repair improve renal tubular cell injury in cisplatin-induced AKI [J]. Autophagy, 2025, 21(9): 1927-44.

[14] PABLA N, DONG Z. Cisplatin nephrotoxicity: mechanisms and renoprotective strategies [J]. Kidney Int, 2008, 73(9): 994-1007.

[15] RAMESH G, REEVES W B. TNF-alpha mediates chemokine and cytokine expression and renal injury in cisplatin nephrotoxicity [J]. J Clin Invest, 2002, 110(6): 835-42.
[16] HU Z, ZHANG H, YI B, et al. VDR activation attenuate cisplatin induced AKI by inhibiting ferroptosis [J]. Cell Death Dis, 2020, 11(1): 73.
[17] LI Y, LI K, ZHAO W, et al. VPA improves ferroptosis in tubular epithelial cells after cisplatin-induced acute kidney injury [J]. Front Pharmacol, 2023, 14: 1147772.
[18] XUE X, ZHU X, ZHOU L, et al. The Hippo Coactivator TAZ Exacerbates Cisplatin-Induced Acute Renal Injury [J]. Kidney Dis (Basel), 2024, 10(6): 421-35.
[19] STOCKWELL B R, FRIEDMANN ANGELI J P, BAYIR H, et al. Ferroptosis: A Regulated Cell Death Nexus Linking Metabolism, Redox Biology, and Disease [J]. Cell, 2017, 171(2): 273-85.
[20] MANCIAS J D, WANG X, GYGI S P, et al. Quantitative proteomics identifies NCOA4 as the cargo receptor mediating ferritinophagy [J]. Nature, 2014, 509(7498): 105-9.
[21] HOU W, XIE Y, SONG X, et al. Autophagy promotes ferroptosis by degradation of ferritin [J]. Autophagy, 2016, 12(8): 1425-8.
[22] TAKAHASHI A, KIMURA T, TAKABATAKE Y, et al. Autophagy guards against cisplatin-induced acute kidney injury [J]. Am J Pathol, 2012, 180(2): 517-25.
[23] KLIONSKY D J, ABDEL-AZIZ A K, ABDELFATAH S, et al. Guidelines for the use and interpretation of assays for monitoring autophagy (4th edition) [J]. Autophagy, 2021, 17(1): 1-382.
[24] HAN M, GUAN Q, YAN F, et al. Disruption of FGL2 induces TFEB-dependent lysosomal degradation of PD-L1 and enhances the efficacy of anti-PD1 therapy in hepatocellular carcinoma [J]. Cell Commun Signal, 2026, 24(1).

Figures and Figure legends

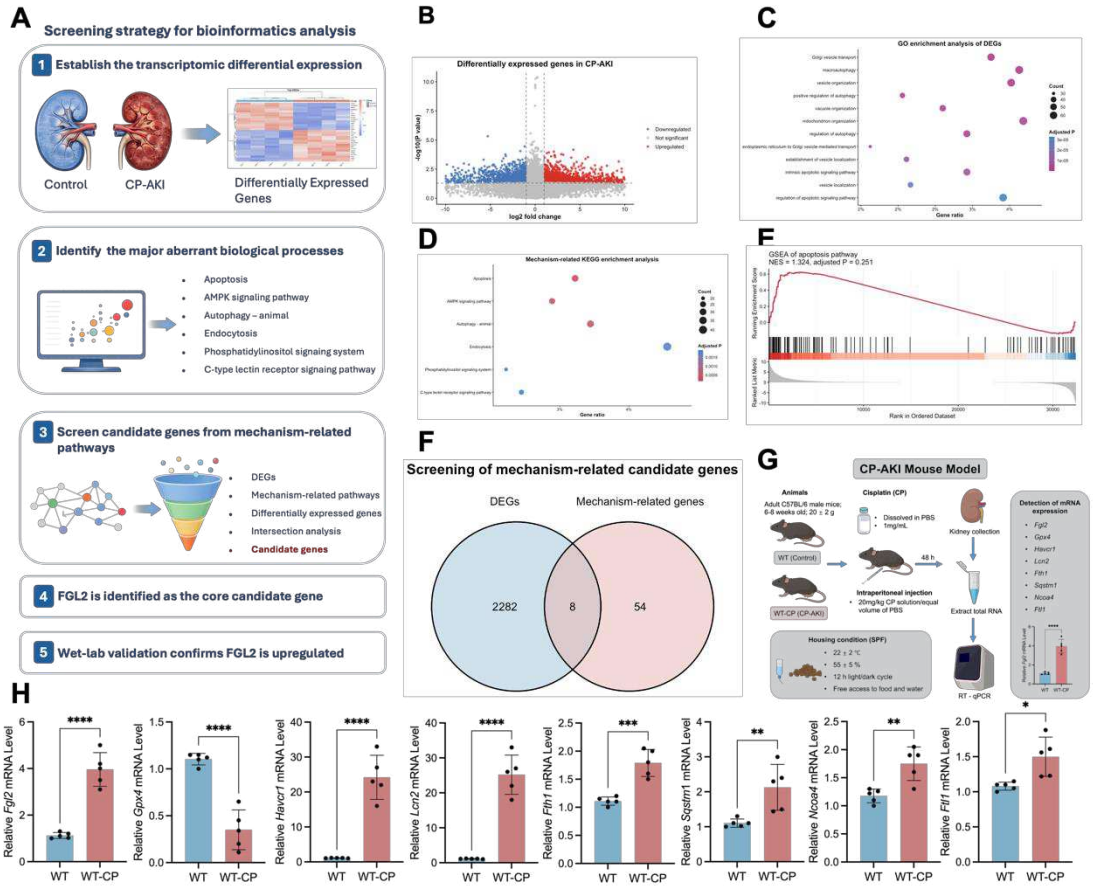


Figure 1. Transcriptomic screening and experimental assessment of FGL2 expression in cisplatin-induced acute kidney injury

(A) Workflow for identifying candidate genes associated with cisplatin-induced CP-AKI using transcriptomic analysis and experimental validation;

(B) Volcano plot showing DEGs between control and cisplatin-treated kidney samples. Red and blue dots indicate upregulated and downregulated genes, respectively;

(C) GO enrichment analysis of DEGs, showing the distribution of enriched biological processes;

(D) KEGG pathway analysis highlighting selected pathways associated with the transcriptional response to cisplatin;

(E) GSEA of the apoptosis pathway (NES = 1.324, adjusted P = 0.251);

(F) Venn diagram showing eight genes shared between the DEGs and a predefined set of mechanism-related genes;

(G) Experimental design for the cisplatin-induced AKI mouse model and subsequent analysis of renal gene expression;

(H) Relative renal mRNA levels of *Fgl2*, *Gpx4*, *Havcr1*, *Lcn2*, *Fth1*, *Sqstm1*, *Ncoa4*, and *Ftl1* in control and cisplatin-treated wild-type mice, determined by RT-qPCR.

*Data are presented as mean ± SD (n = 5 mice per group). *P < 0.05, **P < 0.01, ***P < 0.001, and ****P < 0.0001.*

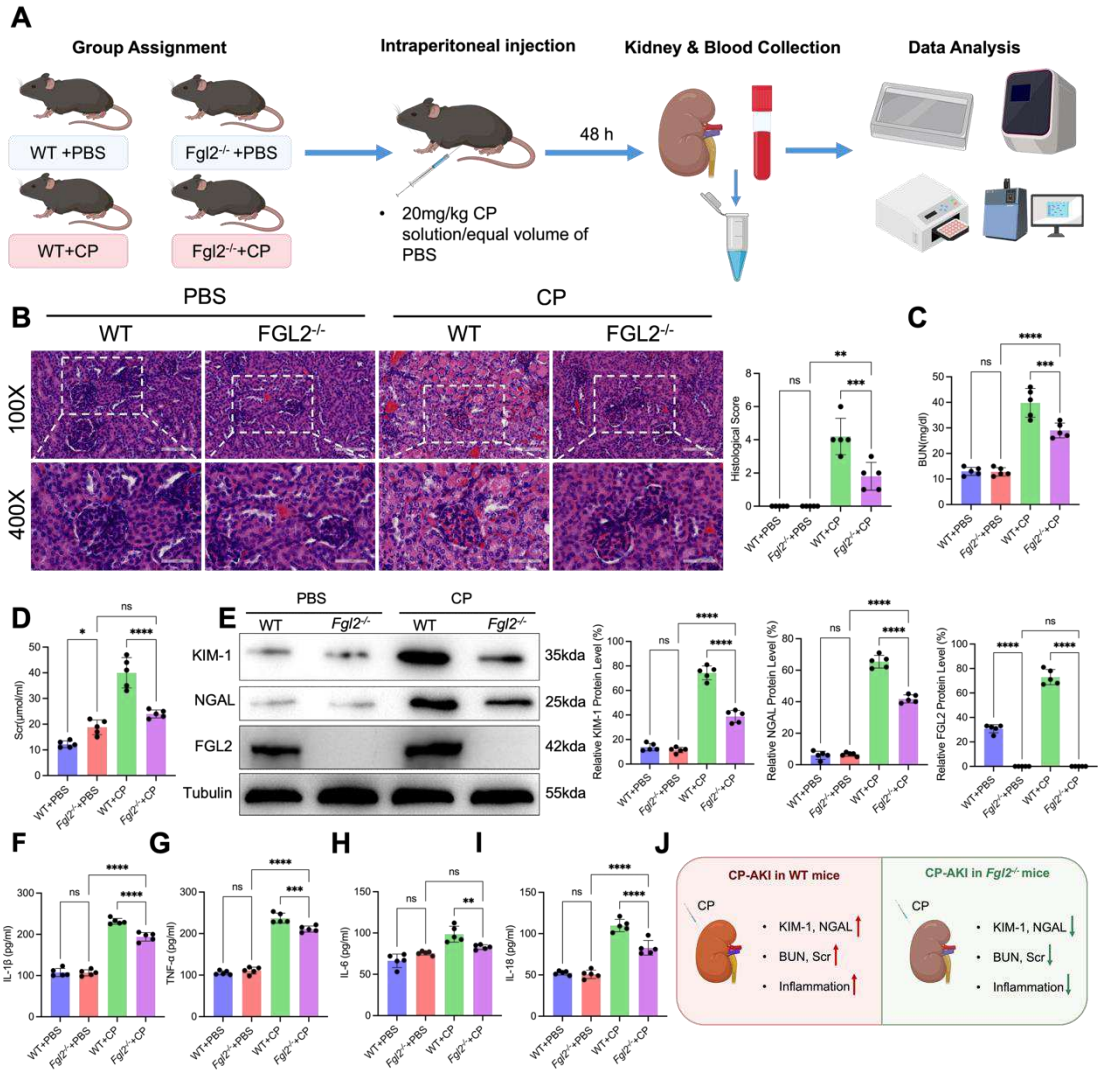


Figure 2. FGL2 deficiency attenuates cisplatin-induced renal injury and inflammation *in vivo*.

(A) Experimental design. WT and Fgl2$^{-/-}$ mice received intraperitoneal injections of PBS or cisplatin (20 mg/kg). Blood and kidney samples were collected 48 h later;

(B) Representative H&E-stained kidney sections at 100× and 400× magnification, with quantification of tubular injury scores. Dashed boxes indicate the enlarged regions;

(C, D) BUN and Scr levels, respectively;

(E) Western blot analysis of KIM-1, NGAL, and FGL2 in kidney tissues, with tubulin as the loading control. Relative protein levels were quantified by densitometry;

(F–I) Levels of the inflammatory cytokines IL-1β, TNF-α, IL-6, and IL-18 in the indicated groups;

(J) Schematic summary of renal injury and inflammatory changes in cisplatin-treated WT and Fgl2$^{-/-}$ mice.

*Data are presented as mean ± SD (n = 5 mice per group). Statistical comparisons were performed using two-way ANOVA followed by Tukey's multiple-comparison test. ns, not significant; *P < 0.05, **P < 0.01, ***P < 0.001, and ****P < 0.0001.*

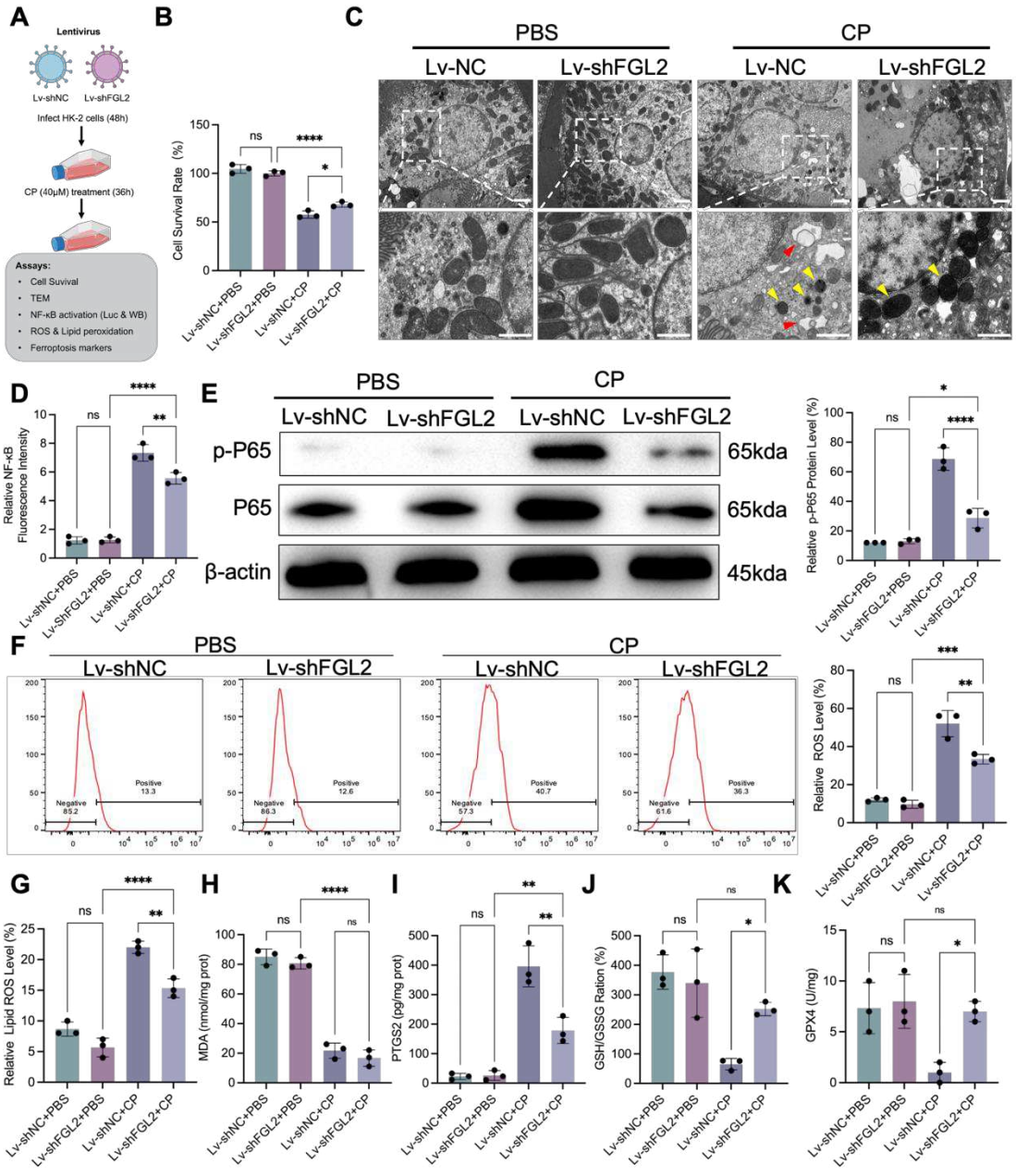


Figure 3. FGL2 knockdown attenuates cisplatin-induced cellular injury and oxidative stress in HK-2 cells

(A) Experimental design. HK-2 cells transduced with Lv-shNC or Lv-shFGL2 were treated with PBS or cisplatin (40 μM) for 36 h;

(B) Cell viability measured by the CCK-8 assay;

(C) Representative TEM images showing mitochondrial ultrastructural changes after cisplatin exposure. Yellow arrows indicate damaged mitochondria;

(D) Relative NF-κB transcriptional activity in HK-2 cells under the indicated treatment conditions;

(E) Western blot analysis of p-p65 and total p65, with β-actin as the loading control. Relative protein levels were quantified by densitometry;

(F) Flow cytometric measurement of intracellular ROS, with corresponding quantitative analysis;

(G) Lipid ROS levels in HK-2 cells;

(H) MDA levels;

(I) PTGS2 levels;

(J) GSH/GSSG ratios;

(K) GPX4 activity.

*Data are presented as mean ± SD (n = 3). Statistical comparisons were performed using two-way ANOVA followed by Tukey's multiple-comparison test. ns, not significant; *P < 0.05, **P < 0.01, ***P < 0.001, and ****P < 0.0001.*

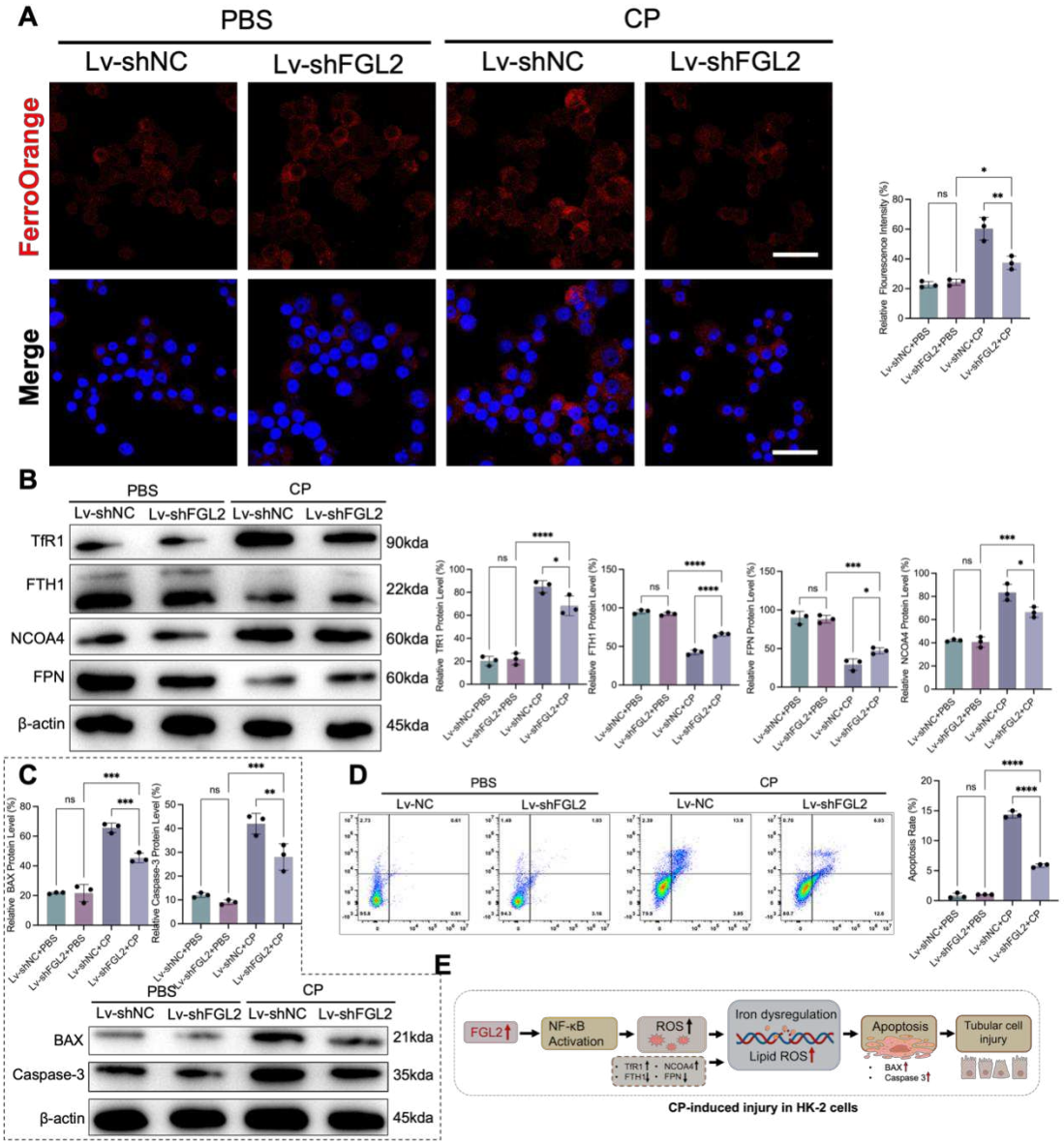


Figure 4. FGL2 knockdown attenuates iron homeostasis alterations and apoptosis in cisplatin-treated HK-2 cells.

(A) Representative FerroOrange fluorescence images showing intracellular labile Fe^{2+} in HK-2 cells following FGL2 knockdown and cisplatin treatment, with quantification of relative fluorescence intensity. Nuclei were counterstained with DAPI;

(B) Western blot analysis of iron metabolism-related proteins, including TfR1, FTH1, NCOA4, and FPN, with corresponding densitometric quantification;

(C) Western blot analysis of BAX and caspase-3 expression and relative protein levels. β-actin served as the loading control;

(D) Flow cytometric analysis and quantification of late apoptotic cells (Annexin V-positive/PI-positive, upper-right quadrant) in each group;

(E) Schematic overview of FGL2-associated changes in iron metabolism, oxidative stress, NF-κB signaling, and apoptosis following cisplatin exposure.

*Data are presented as mean ± SD (n = 3). Statistical comparisons were performed using two-way ANOVA followed by Tukey's multiple-comparison test. ns, not significant; *P < 0.05, **P < 0.01, ***P < 0.001, and ****P < 0.0001.*

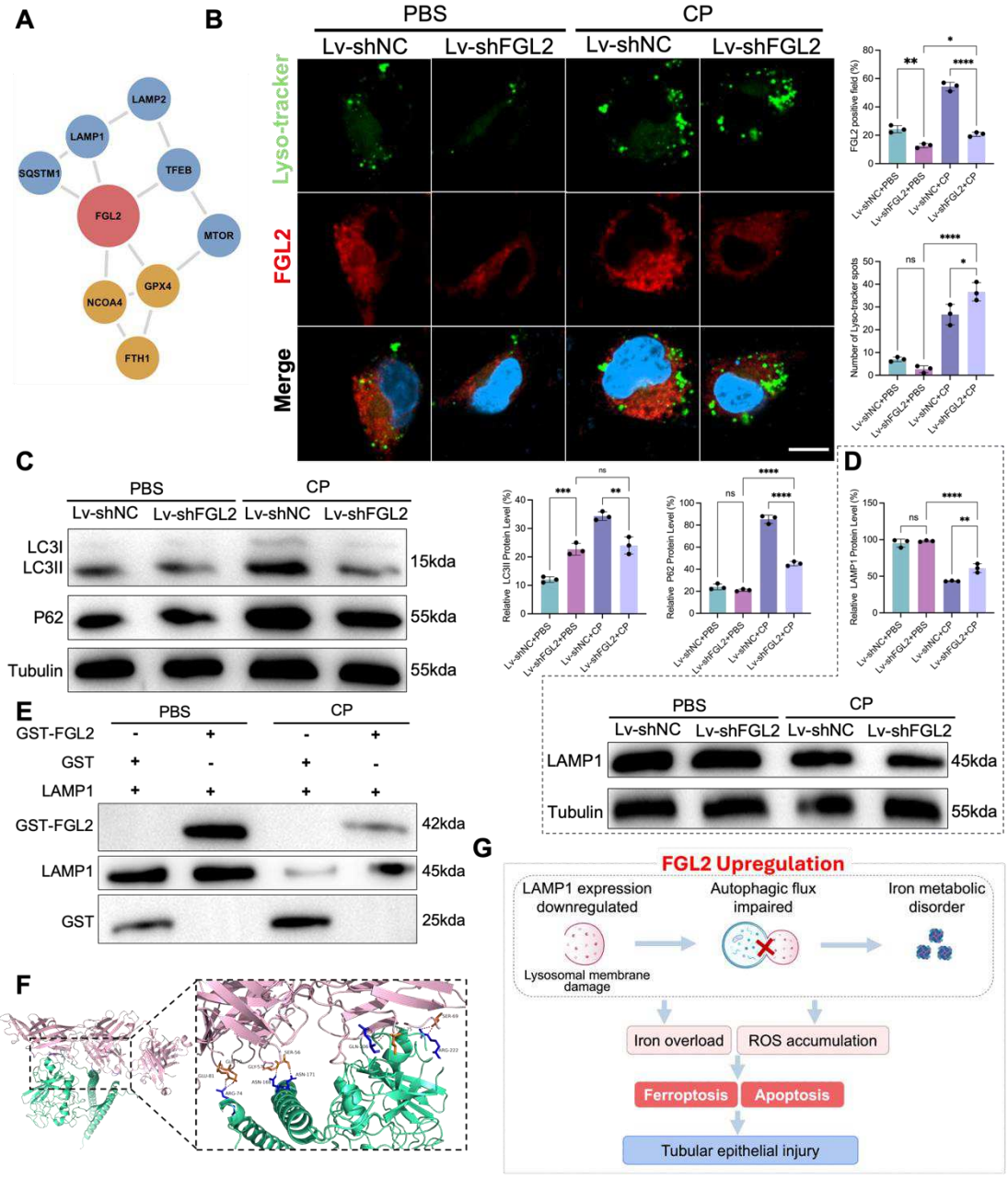


Figure 5. FGL2 knockdown attenuates lysosomal and autophagy-related alterations in cisplatin-treated HK-2 cells.

(A) Protein–protein interaction network showing predicted functional associations between FGL2 and lysosome- or autophagy-related proteins, including LAMP1, LAMP2, SQSTM1, TFEB, mTOR, GPX4, NCOA4, and FTH1;

(B) Representative fluorescence images of LysoTracker (green) and FGL2 (red) in HK-2 cells following FGL2 knockdown and cisplatin treatment. Nuclei were counterstained with DAPI (blue). FGL2-positive areas and LysoTracker-positive puncta were quantified;

(C) Western blot analysis of LC3-I/II and p62, with tubulin as the loading control. Relative protein levels were determined by densitometry;

(D) Western blot analysis and quantification of LAMP1 expression in the indicated groups. (E) GST pull-down assay examining LAMP1 recovery in GST-FGL2 and GST-only fractions under the indicated conditions;

(F) Molecular docking model of the potential FGL2–LAMP1 interaction, with an enlarged view of the predicted interface;

(G) Schematic illustration of the proposed relationships between FGL2 upregulation, lysosomal alterations, disturbed iron homeostasis, oxidative stress, and tubular epithelial injury.

*Data are presented as mean ± SD (n = 3). Statistical comparisons were performed using two-way ANOVA followed by Tukey's multiple-comparison test. ns, not significant; *P < 0.05, **P < 0.01, ***P < 0.001, and ****P < 0.0001.*

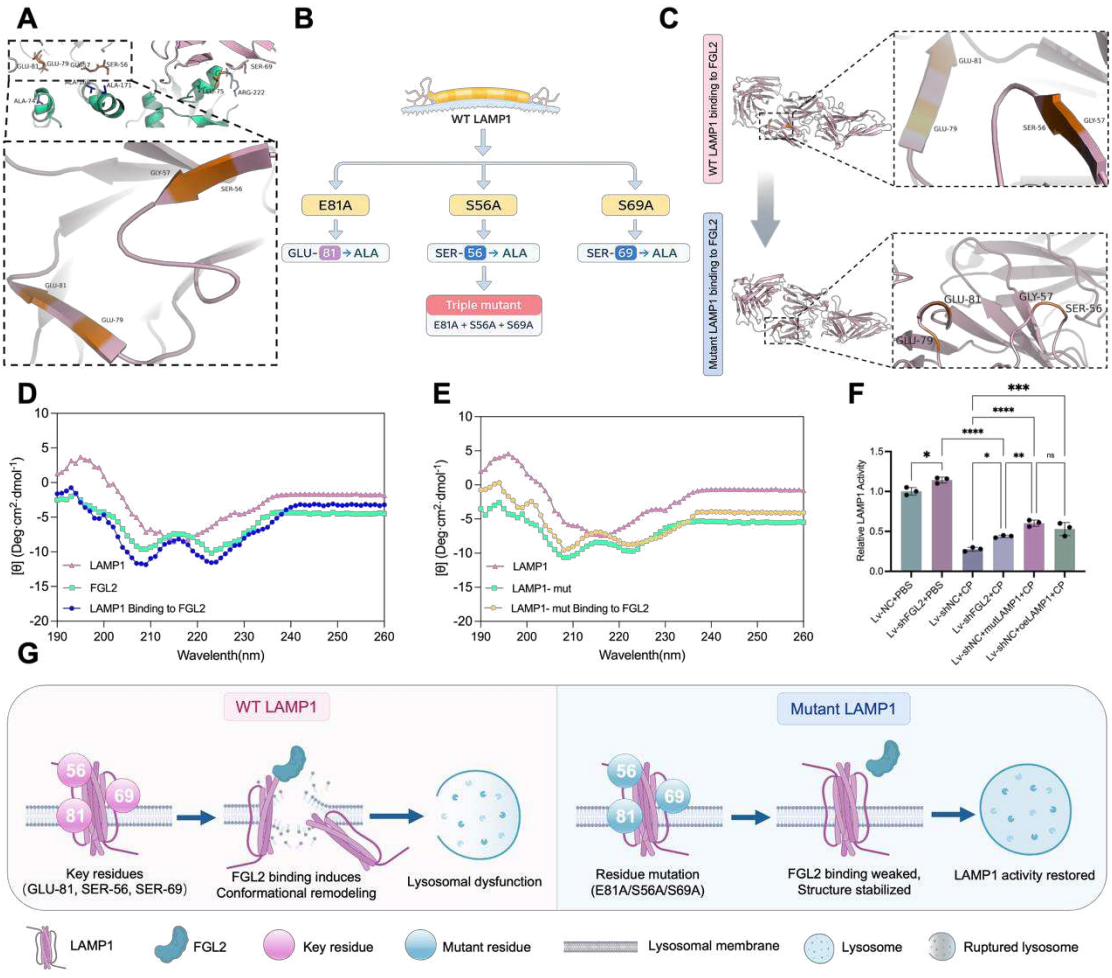


Figure 6. Structural analysis of LAMP1 variants at a predicted FGL2–LAMP1 interaction interface.

(A) Molecular docking model of FGL2 and LAMP1, highlighting the predicted interface and candidate LAMP1 residues E81, S56, and S69;

(B) Design of LAMP1 mutants carrying individual alanine substitutions (E81A, S56A, and S69A) or all three substitutions;

(C) Comparison of predicted docking configurations involving wild-type and mutant LAMP1, with enlarged views of the candidate interface;

(D, E) CD spectra of the indicated protein samples and their mixtures, showing differences in spectral profiles;

(F) Quantification of the LAMP1-associated assay readout in the indicated treatment groups;

(G) Schematic representation of the proposed relationship between FGL2, LAMP1 structural alterations, and lysosomal homeostasis. The predicted interaction and its functional consequences remain to be experimentally established.

*Quantitative data are presented as mean ± SD (n = 3). ns, not significant; *P < 0.05, **P < 0.01, and ***P < 0.001.*

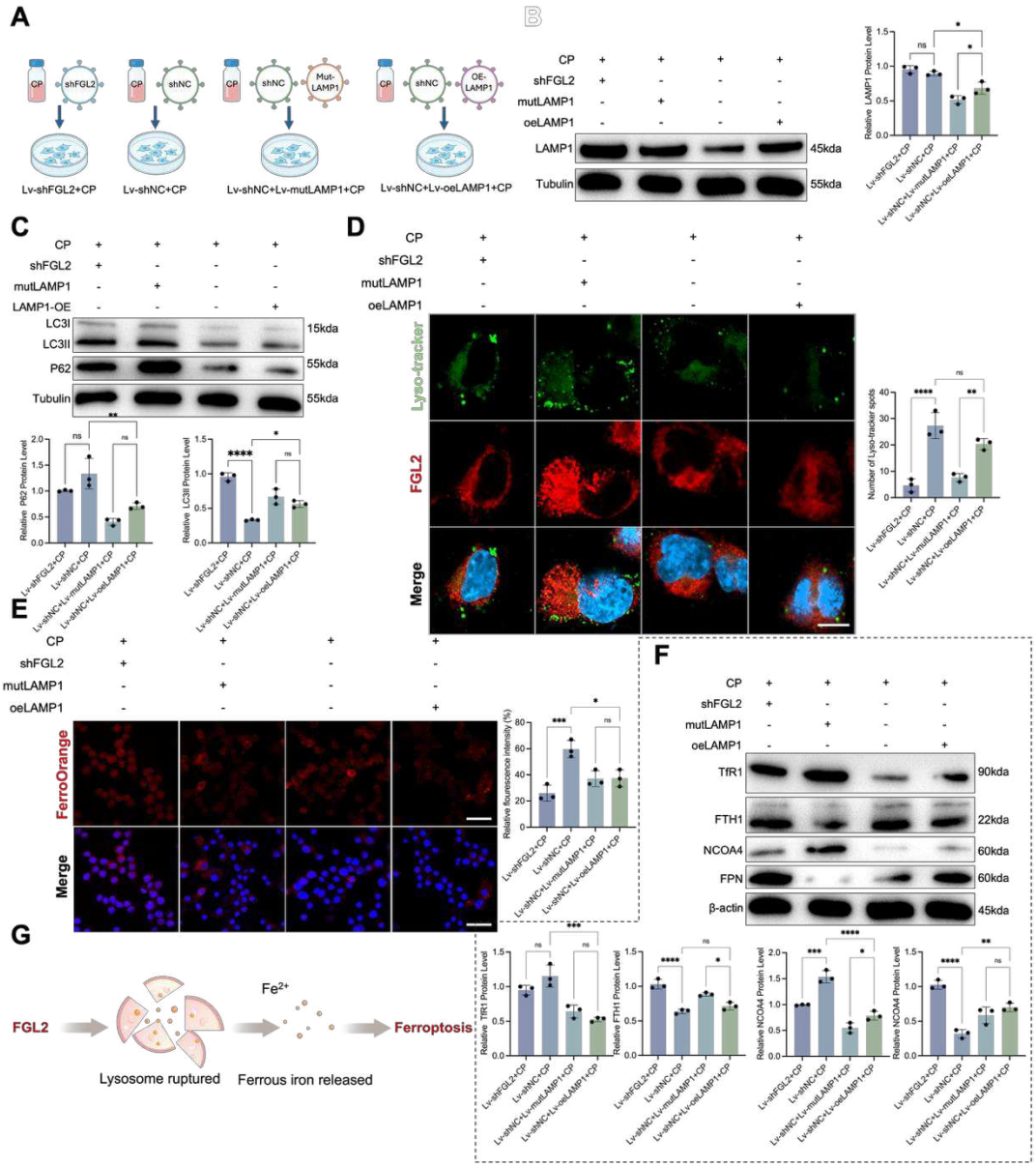


Figure 7. Changes in lysosome-associated markers and iron homeostasis following LAMP1 modulation in cisplatin-treated HK-2 cells.

(A) Experimental design showing HK-2 cells exposed to cisplatin (CP) under the indicated FGL2 knockdown, LAMP1 overexpression, or mutant LAMP1 conditions;

(B) Western blot analysis of LAMP1 expression, with tubulin as the loading control. Protein levels were quantified by densitometry;

(C) Western blot analysis of LC3-I/II and p62, with corresponding quantification of relative protein levels;

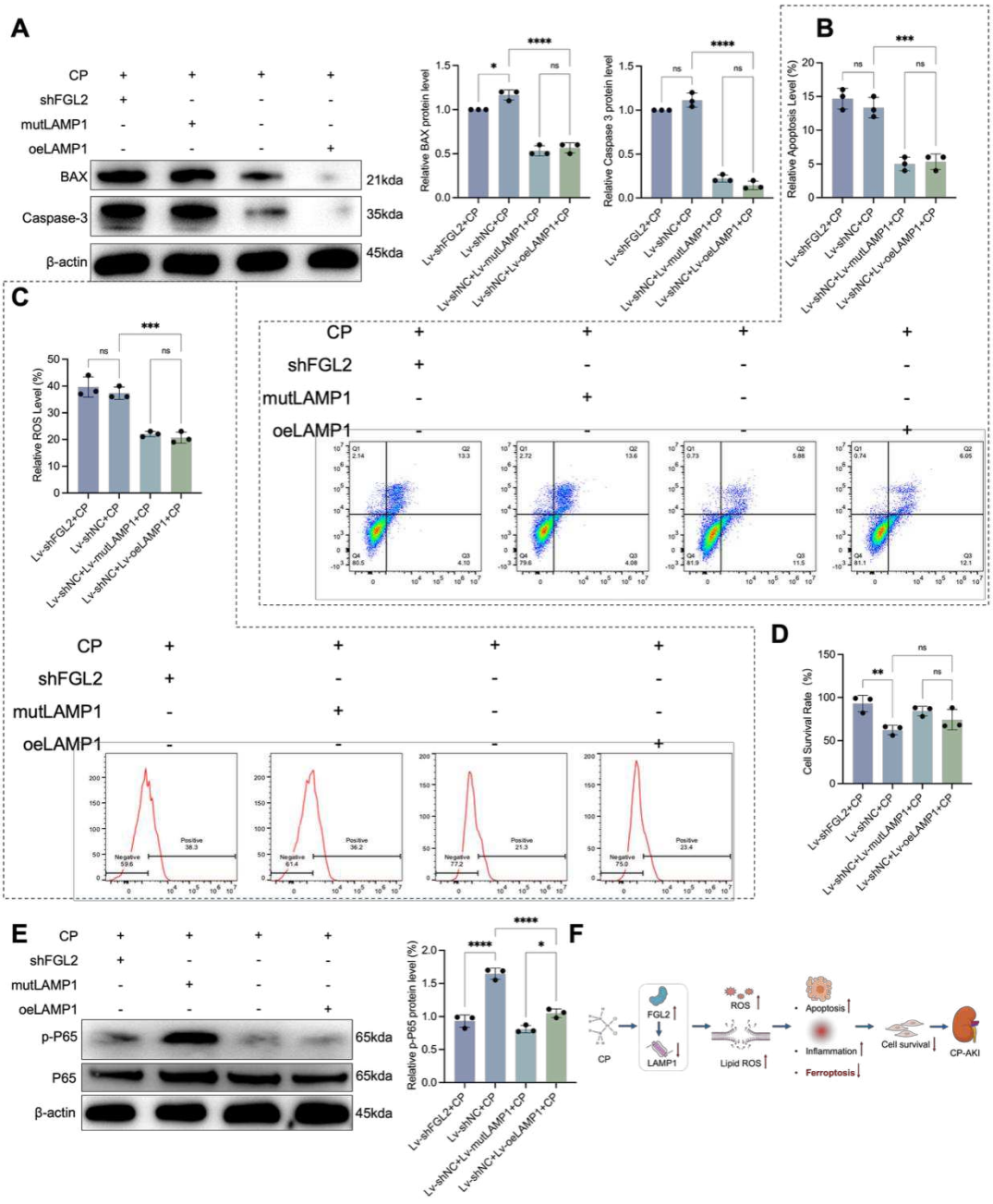
(D) Representative fluorescence images of LysoTracker (green) and FGL2 (red) staining, with DAPI nuclear counterstaining (blue). LysoTracker fluorescence was quantified in each group. (E)

FerroOrange staining of intracellular labile Fe^{2+}, with quantification of relative fluorescence intensity;

(F) Western blot analysis of iron metabolism-related proteins, including TfR1, FTH1, NCOA4, and FPN, with corresponding densitometric analysis;

(G) Schematic illustration of the proposed association between FGL2-related lysosomal alterations, disturbed iron homeostasis, and ferroptosis-associated cellular responses.

*Data are presented as mean ± SD (n = 3). ns, not significant; *P < 0.05, **P < 0.01, ***P < 0.001, and ****P < 0.0001.*



935

936 **Figure 8. FGL2 knockdown and LAMP1 modulation are associated with reduced apoptosis,**
937 **oxidative stress, and NF-κB signaling in cisplatin-treated HK-2 cells.**

938 (A) Western blot analysis of BAX and caspase-3, with β-actin as the loading control. Relative
939 protein levels were quantified by densitometry;

940 (B) Quantification of late apoptotic cells in the indicated treatment groups;

941 (C) Representative flow cytometric plots showing apoptotic cell populations and intracellular ROS
942 signals under the indicated treatment conditions;

943 (D) Quantification of relative cell survival in the indicated groups;

(E) Western blot analysis of p-p65 and total p65, with corresponding densitometric quantification. β-actin served as the loading control;

(F) Schematic overview of the proposed relationships between FGL2, LAMP1, oxidative stress, inflammatory signaling, and cisplatin-associated renal injury.

*Quantitative data are presented as mean ± SD (n = 3). ns, not significant; *P < 0.05, **P < 0.01, ***P < 0.001, and ****P < 0.0001.*